Vibronic Coupling in the Ground and Excited States of Oligoacene Cations†

Roel S. Sánchez-Carrera,‡ Veaceslav Coropceanu,*,‡ Demetrio A. da Silva Filho,‡ Rainer Friedlein,§ Wojciech Osikowicz,§ Richard Murdey,§,|| Christian Suess,§ William R. Salaneck,§ and Jean-Luc Brédas*,‡

School of Chemistry and Biochemistry, Georgia Institute of Technology, Atlanta, Georgia 30332-0400, and Department of Physics, Linköping University, S-581 83 Linköping, Sweden

Received: December 22, 2005; In Final Form: May 4, 2006

The vibrational coupling in the ground and excited states of positively charged naphthalene, anthracene, tetracene, and pentacene molecules is studied on the basis of a joint experimental and theoretical study of ionization spectra using high-resolution gas-phase photoelectron spectroscopy and first-principles correlated quantum-mechanical calculations. Our theoretical and experimental results reveal that, while the main contribution to relaxation energy in the ground state of oligoacene systems comes from high-energy vibrations, the excited-state relaxation energies show a significant redistribution toward lower-frequency vibrations. A direct correlation is found between the nature of the vibronic interaction and the pattern of the electronic state structure.

1. Introduction

Oligoacenes play an important role in many areas of chemistry, materials science, and astrophysics. For instance, oligoacene radical cations are thought to be responsible for interstellar infrared emission features and diffuse interstellar visible absorption bands.[1−6] Oligoacenes are also among the most studied organic materials[7−13] used as active elements in new generations of organic (opto)electronic devices. A detailed understanding of the properties of oligoacenes and their derivatives is thus of interest from both fundamental and practical points of view.

Vibronic coupling represents a key interaction that can control to a large extent many system properties such as the profile of the optical bands, superconductivity, or the efficiency of charge and energy transport.[8] Vibronic coupling in oligoacenes has been previously addressed in several theoretical and experimental studies.[1,8,14−34] In recent work, we investigated the relaxation processes in the radical-cation ground state upon positive ionization of anthracene, tetracene, and pentacene; these were studied using an approach that combines high-resolution gas-phase photoelectron (PE) spectroscopy measurements with first-principles quantum-mechanical calculations.[28−30] In a more recent communication,[31] we have shown that this approach can be applied as well to study the vibronic interaction in the excited states; up to now, however, these investigations have been limited to naphthalene. Here, on the basis of results obtained for naphthalene, anthracene, tetracene, and pentacene, we discuss the dependence of the hole−vibrational interaction on the molecular size in both ground and excited states. We have also investigated how the amount of "exact" Hartree−Fock exchange (EEX)[15] included in hybrid functionals affects density functional theory (DFT) results and the reliability of DFT to reproduce experimental findings.

2. Experimental Section

The gas-phase PE spectra of naphthalene and anthracene were obtained using 60 eV photons from the MAX-II storage ring at the MAX-Lab synchrotron radiation facility in Lund, Sweden. The Scienta SES-200 photoelectron spectrometer of beamline I411 was tuned to the magic angle between the electric field vector of the light and the direction of the photoelectron emission. An overall resolution of about 26 meV was employed. For naphthalene, a gas cell with an external feed was used allowing high gas densities (local pressure $> 1 \times 10^{-5}$ mbar) and moderate temperatures of 40 ± 20 °C in the target zone. Anthracene spectra have been measured on a stream of molecules from a home-built, externally feedable Knudsen cell (pressure on the order of 10^{-6} mbar, temperature 100 ± 30 °C).

3. Theoretical Methodology

Figure 1 represents the potential energy surfaces for electronic states 1 and 2 corresponding to the neutral state and the ground or excited cation state of the molecule; the geometry relaxation energies upon vertical transition from the neutral state to a charged state and vice versa ($\lambda_{rel}^{(1)}$, $\lambda_{rel}^{(2)}$) are given by

$$\lambda_{rel}^{(1)} = E^{(1)}(M) - E^{(0)}(M) \quad (1)$$

$$\lambda_{rel}^{(2)} = E^{(1)}(M^{+\bullet}) - E^{(0)}(M^{+\bullet}) \quad (2)$$

Here, $E^{(0)}(M)$ and $E^{(0)}(M^{+\bullet})$ are the ground-state energy of the neutral state and the energy of the considered cation state, respectively; $E^{(1)}(M)$ is the energy of the neutral molecule at the optimal cation geometry, and $E^{(1)}(M^{+\bullet})$ is the energy of the cation state at the optimal geometry of the neutral molecule.

The contribution of each vibrational mode to λ_{rel} can be obtained by expanding the potential energies of the neutral and cation states in a power series of the normal coordinates (denoted here as Q_1 and Q_2). In the harmonic approximation, the relaxation energy λ_{rel} is

$$\lambda_{rel} = \sum \lambda_i = \sum \hbar\omega_i S_i \quad (3)$$

$$\lambda_i = \frac{k_i}{2} \Delta Q_i^2 \quad S_i = \lambda_i/\hbar\omega_i \quad (4)$$

† Part of the special issue "Robert J. Silbey Festschrift".

* To whom correspondence should be addressed. E-mail: veaceslav.coropceanu@chemistry.gatech.edu; jean-luc.bredas@chemistry.gatech.edu.

‡ Georgia Institute of Technology.

§ Linköping University.

|| Present address: Institute for Chemical Research, Kyoto University, Uji, Kyoto 611-0011, Japan.

10.1021/jp057462p CCC: $33.50
Published on Web 06/13/2006

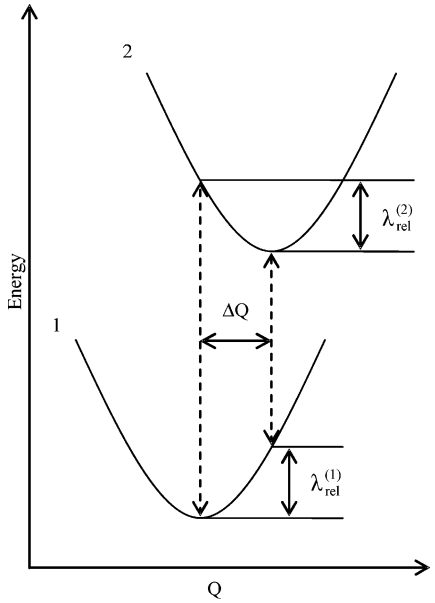

Figure 1. Sketch of the potential energy surfaces for neutral state 1 and cation state 2, showing the vertical transitions (dashed lines), the normal mode displacement ΔQ, and the relaxation energies $\lambda_{rel}^{(1)}$ and $\lambda_{rel}^{(2)}$.

Here, the summations run over the vibrational modes; ΔQ_i represents the displacement along normal mode i between the equilibrium positions of the two electronic states of interest; k_i and ω_i are the corresponding force constants and vibrational frequencies; S_i denotes the Huang−Rhys factor (electron−vibration coupling constant).

We performed geometry optimizations for the neutral and radical-cation states of naphthalene, anthracene, tetracene, and pentacene, followed by calculation of harmonic vibrational frequencies and normal modes. The calculations were achieved at the DFT level using the 6-31G** basis set and the BLYP, B3LYP, and BHandHLYP functionals as implemented in the Gaussian 98 program.[35] For the sake of comparison, calculations have been also performed at the Hartree−Fock (HF) level with the same basis set. Spin-unrestricted wave functions were used for the investigation of the radical-cation states. All excited-state calculations have been achieved by applying symmetry constraints on the wave functions.

The normal modes $\mathbf{Q}_{1(2)}$ obtained from the quantum-mechanical calculations are given as a linear combination of Cartesian displacements

$$\mathbf{Q}_{1(2)} = \sum_j \mathbf{L}_{1(2)ji} (\mathbf{q}_{1(2)j} - \mathbf{q}_{1(2)j}^{(0)}) \quad (5)$$

Here, the matrix $\mathbf{L}_{1(2)}$ connects the $3n - 6$ (n is the number of atoms in the (nonlinear) molecule) normal coordinates with the set of $3n$ mass-weighted Cartesian coordinates $q_{1(2)}$; the vectors $\mathbf{q}_1^{(0)}$ and $\mathbf{q}_2^{(0)}$ correspond to the stationary points on the adiabatic potential surfaces of states 1 and 2, respectively. The normal mode displacements $\Delta\mathbf{Q}_{1(2)}$ are obtained by projecting the displacements $\Delta q = q_1^{(0)} - q_2^{(0)}$ onto the normal mode vectors. The Huang−Rhys factors and the total relaxation energy are then obtained then by using eqs 3 and 4. It is important to note that the normal modes of the neutral and cation states, $\mathbf{Q}_1$ and $\mathbf{Q}_2$, are in general different and are related by the Duschinsky matrix, $\mathbf{J}$, as[36]

$$\mathbf{Q}_1 = \mathbf{J}\mathbf{Q}_2 + \Delta\mathbf{Q} \quad (6)$$

The calculations of the Huang−Rhys factors and Duschinsky matrices have been carried out with the DUSHIN program developed by Reimers.[36] For the present system the Duschinsky mixing is found to be minor, and we neglected this effect in the following analyses.

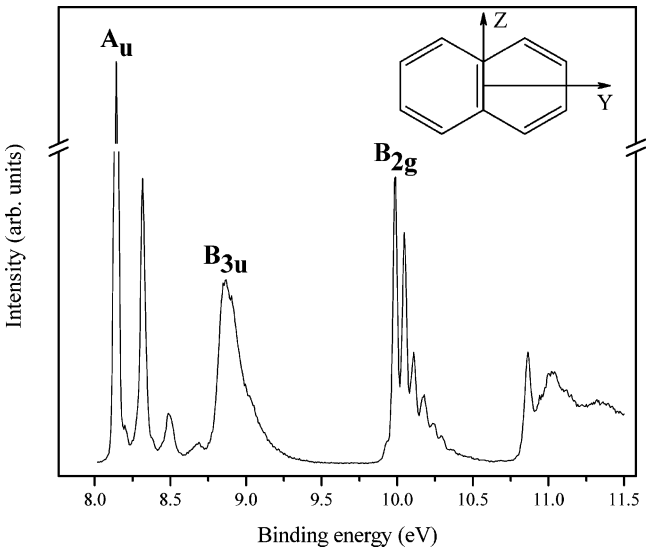

Figure 2. Gas-phase photoelectron emission spectrum of naphthalene.

As in our previous investigations, the simulation of the ionization bands has been performed in the framework of the Born−Oppenheimer and Franck−Condon (FC) approximations.[30] In cases where Duschinsky mixing can be neglected, the relative intensity of a multidimensional vibrational transition, involving p vibrational modes, is obtained as a simple product of one-dimensional FC integrals, $\mathrm{FCI}(m,n) = \langle\Phi_m(Q)\Phi_n(Q)\rangle$ (where $\Phi_m(Q)$ and $\Phi_n(Q)$ are the vibrational functions corresponding to the neutral and cation electronic states)

$$I(m_1,n_1,...,m_p,n_p) = \prod_{i=1}^{p} \mathrm{FCI}(m_1,n_1)^2 \exp\left\{\frac{-\hbar m_1 \omega_i}{k_B T}\right\} \quad (7)$$

$$\mathrm{FCI}(m,n)^2 = \exp\{-S\} S^{(n-m)} \frac{m!}{n!} [L_m^{(n-m)}(S)]^2 \quad (8)$$

where m_i and n_i are the initial and final vibrational quantum numbers of mode Q_i and $L_n^{(m)}$ is a Laguerre polynomial.

4. Results and Discussion

Photoelectron Spectroscopy. The gas-phase photoelectron spectra of naphthalene and anthracene are shown in Figures 2 and 3, respectively. In general, the spectra are similar to those previously reported;[29,37−41] however, the use of synchrotron sources allows the individual peaks in the vibrational fine structure to have a better resolution. The first ionization band of both naphthalene and anthracene exhibits a high-frequency progression of about 1500 cm^{-1}, which lies in the region expected for C−C stretching modes. However, in contrast to anthracene, a contribution from a second vibration at about 500 cm^{-1} is also clearly resolved[31] in naphthalene. In addition, as seen from the profile of the third ionization, the interaction with this mode completely dominates the geometrical relaxation of the $^2B_{2g}$ state of naphthalene upon ionization. In striking contrast to the first and third ionization bands, the second PE band in naphthalene is rather structureless. The second ionization of anthracene, however, exhibits a well-resolved frequency progression of about 750 cm^{-1}. A vibrational structure, although less resolved, is also seen in the third PE band of anthracene.

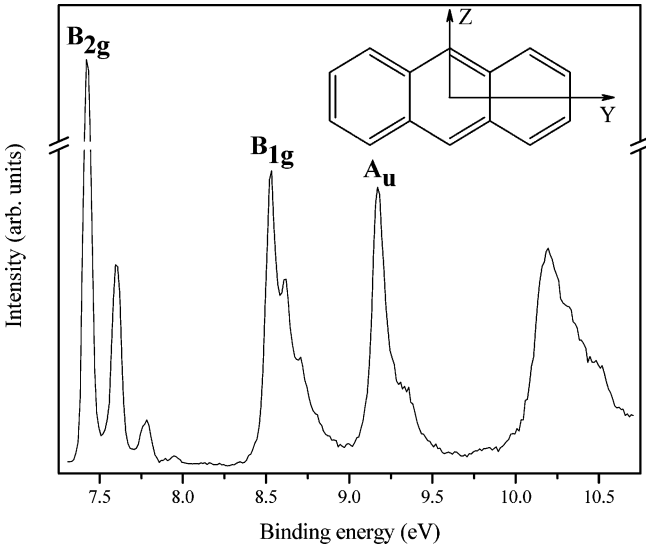

Figure 3. Gas-phase photoelectron emission spectrum of anthracene.

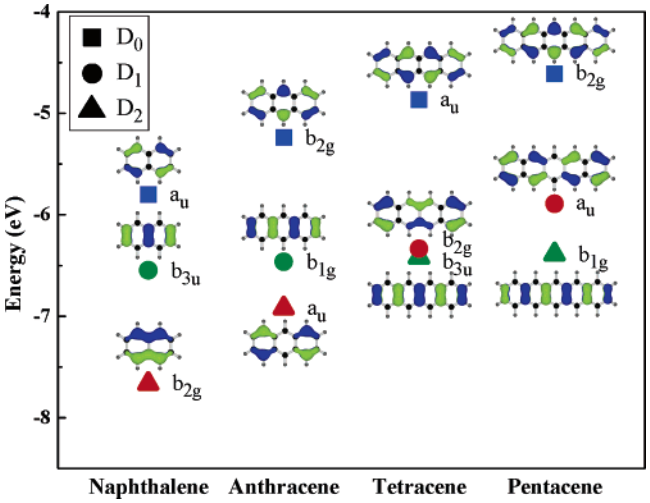

Figure 4. Orbital energies (DFT/B3LYP) of the first free frontier occupied MOs in naphthalene, anthracene, tetracene, and pentacene. The blue, green, and red colors are used to group the MOs by their type (I, II, and III, respectively; see text).

Electronic Structure. The vertical ionization energies of the first three photoelectron bands obtained within the framework of Koopmans' theorem[42] (KT) and at the ΔSCF (self-consistent field) level are collected in Table 1. The KT/HF calculations yield better absolute values for the ionization energies. However, the relative positions of the ionization peaks are better described at the KT/B3LYP level. The B3LYP molecular orbitals (MOs) associated with the first three PE bands are shown in Figure 4. An inspection of Figure 4 reveals that the electron density pattern for the highest occupied MO (HOMO) is the same (we denote it as type I) for all four molecules. The electronic structure of the HOMO − 1 and HOMO − 2 levels with either b_{3u} or b_{1g} symmetry also share a common pattern (type II) along the series. The HOMO − 1 and HOMO − 2 levels with b_{2g} and a_u symmetries are denoted as a type III. Each group of orbitals, as clearly seen from Figure 4, shows a characteristic dependence of their energies on the system size. The second and third ionizations in naphthalene and anthracene, according to the KT calculations, are of type II and type III, respectively; this sequence is inverted in pentacene. The KT results are conflicting for tetracene; while the KT/BLYP and KT/B3LYP calculations yield the $^2B_{2g}$ and $^2B_{3u}$ states (type III and type II) as second and third PE bands, respectively, the KT/BHandHLYP and KT/HF calculations give the opposite ordering. At the ΔSCF level, the B3LYP and BHandHLYP calculations give almost identical results for the first ionization. B3LYP, however, better describes the energy spacing between the excited states. In the cases of naphthalene, anthracene, and pentacene, all three functionals yield the same ordering of the cation states. For tetracene, however, as in the case of the KT calculations, the situation is less clear: The B3LYP calculations yield the $^2B_{2g}$ and $^2B_{3u}$ sequence for the second and third ionizations while the reverse ordering is obtained at the BHandHLYP level. Furthermore, the results of the normal mode calculations reveal that the optimized geometries of the $^2B_{3u}$ state obtained at both B3LYP and BHandHLYP levels correspond to a transition state, which suggests a broken-symmetry effect. In contrast, the BLYP and HF calculations yield a minimum for this state. Further calculations are therefore needed to shed more light on the ordering of the second and third radical-cation states in tetracene and on the shapes of their adiabatic potential surfaces. Finally, we note that our results clearly indicate that ΔSCF/HF calculations, in contrast to DFT calculations, totally fail to describe the PE spectra. This failure is more likely related to large spin

TABLE 1: First Three Ionization Energies (in eV) in Naphthalene, Anthracene, Tetracene, and Pentacene Obtained from ΔSCF and KT (in Parentheses) Calculations

	BLYP	B3LYP	BHandHLYP	HF	experiment
			Naphthalene		
D_0 (^2A_u)	7.39 (4.89)	7.70 (5.80)	7.68 (6.75)	6.92 (7.81)	8.15[b]
D_1 ($^2B_{3u}$)	8.16 (5.59)	8.46 (6.55)	8.39 (7.53)	7.33 (8.54)	8.87[b]
D_2 ($^2B_{2g}$)	9.11 (6.51)	9.61 (7.66)	9.86 (8.92)	9.49 (10.32)	10.08[b]
			Anthracene		
D_0 ($^2B_{2g}$)	6.58 (4.40)	6.89 (5.24)	6.87 (6.08)	6.14 (7.01)	7.42[c]
D_1 ($^2B_{1g}$)	7.78 (5.55)	8.13 (6.46)	8.10 (7.38)	7.03 (8.29)	8.53[c]
D_0 (^2A_u)	8.05 (5.86)	8.59 (6.92)	8.91 (8.06)	8.72 (9.35)	9.17[c]
			Tetracene		
D_0 (^2A_u)	6.04 (4.09)	6.34 (4.87)	6.31 (5.63)	5.58 (6.47)	6.94[c]
D_1 ($^2B_{2g}$)	7.28 (5.35)	7.82 (6.34)	8.15 (7.37[a])	8.01 (8.52)[a]	8.30−8.40[c]
D_2 ($^2B_{3u}$)	7.52 (5.53)	(6.42)	(7.29[a])	6.83 (8.13)[a]	8.40−8.60[c]
			Pentacene		
D_0 ($^2B_{2g}$)	5.65 (3.88)	5.95 (4.61)	5.91 (5.31)	5.18 (6.08)	6.59[c]
D_1 (^2A_u)	6.72 (4.97)	7.23 (5.89)	7.54 (6.84)	7.39[a](7.88)	7.89[c]
D_2 ($^2B_{1g}$)	7.32 (5.52)	7.74 (6.39)	7.78 (7.23)	6.67[a](8.03)	8.27[c]

[a] In these results the ordering of the D_1 and D_2 states (and/or of the respective MO) is inversed. [b] Taken from ref 41. [c] Derived from the data published in ref 29.

TABLE 2: Adiabatic Potential (AP) Surfaces and Normal Mode (NM) Estimates of the Relaxation Energies λ_{rel} (meV) of the Cation States D_0, D_1, and D_2 of Naphthalene, Anthracene, Tetracene, and Pentacene, Related to Ionization Processes

	BLYP		B3LYP		BHandHLYP		HF	
	AP	NM	AP	NM	AP	NM	AP	NM
				Naphthalene				
D_0	72	70	91	91	133	130	243	236
D_1	98	92	110	103	127	119	152	141
D_2	126	122	133	128	144	141	168	165
				Anthracene				
D_0	50	49	68	68	110	112	222	223
D_1	76	73	88	85	107	102	138	130
D_2	68	67	77	75	91	90	126	125
				Tetracene				
D_0	38	37	56	57	97	93	217	211
D_1	49	50	59	59			132	124
D_2	63	61			78	77	128	125
				Pentacene				
D_0	30	31	48	48	88	90	229	228
D_1	39	38	49	47	66	65	112	110
D_2	53	52	64	63	84	81	134	128

contaminations observed in the (unrestricted) HF calculations of the radical-cation states, in particular the excited states.

Relaxation Energy. The results of the DFT and HF calculations of the relaxation energies in naphthalene, anthracene, tetracene, and pentacene related to the first three PE bands; i.e., the geometry relaxations in the radical-cation states D_0, D_1, and D_2 are reported in Table 2 for both the adiabatic potential (AP) surface and the normal mode (NM) approaches. The partition of the reorganization energy into the contributions of each normal mode for anthracene is given in Table 3 (see the Supporting Information for the corresponding data for the other systems).

Our results are in line with recent findings by Dierkesen and Grimme[15] and indicate that the calculated value of λ_{rel} crucially depends on the amount of EEX included in the hybrid functionals. As seen from Table 2, the values of λ_{rel} derived at the DFT level are much smaller than the values obtained at the HF level. The DFT estimates of λ_{rel} increase with the increase in EEX contribution to the hybrid functionals: λ_{rel}(BLYP, 0% EEX) < λ_{rel}(B3LYP, 20% EEX) < λ_{rel}(BHandHLYP, 50% EEX). Our results show that the dependence of λ_{rel} on the EEX amount is state-dependent. For instance, the ratio λ_{rel}(HF)/λ_{rel}(BLYP) is at least twice as large for the D_0 state as those for the first two excited radical-cations states D_1 and D_2. Moreover, as seen from Table 3 (see also Figure S2 in the Supporting Information), the contributions of each vibration to λ_{rel} do not scale in the same way for all vibrations when going from one functional to another but are rather mode-dependent.

The relaxation energies obtained at the HF level and DFT level with different functionals (Table 2) show different dependences as a function of system size. For instance, the BLYP values of λ_{rel} for the D_0 state decreases by over a factor of 2 when going from naphthalene to pentacene. The variation of λ_{rel} becomes smaller, however, as the amount of the EEX included in hybrid functionals increases; at the HF level, λ_{rel} is practically independent of molecular size. This trend shown by

TABLE 3: DFT and HF Estimates of Frequencies, ω, and Relaxation Energies, λ_{rel}, of the Cation States D_0, D_1, and D_2, Related to the Ionization of Anthracene

	BLYP		B3LYP		BHandHLYP		HF	
vibrational mode	ω (cm^{-1})	λ_{rel} (meV)	ω (cm^{-1})	λ_{rel} (meV)	ω (cm^{-1})	λ_{rel} (meV)	ω (cm^{-1})	λ_{rel} (meV)
				D_0				
1	385	0	396	0	408	0	416	0
2	612	0	626	0	644	0	661	0
3	741	0	766	0	795	0	813	0
4	1025	0	1057	0	1096	0	1125	1
5	1177	3	1207	4	1245	6	1285	19
6	1254	1	1291	3	1332	7	1352	22
7	1377	16	1426	27	1473	51	1466	111
8	1495	7	1545	9	1607	15	1665	32
9	1546	21	1611	25	1689	32	1756	37
10	3147	0	3228	0	3327	0	3395	0
				D_1				
1	387	7	398	8	411	10	419	7
2	614	2	629	2	648	2	667	3
3	706	32	730	39	759	49	777	66
4	966	12	996	11	1028	11	1023	19
5	1174	3	1206	4	1247	4	1293	3
6	1274	0	1315	0	1362	0	1385	2
7	1390	2	1453	3	1526	7	1566	12
8	1455	3	1499	2	1554	0	1607	1
9	1523	11	1591	14	1673	18	1734	17
10	3147	0	3229	0	3328	0	3396	1
				D_2				
1	383	11	394	11	407	12	417	14
2	617	7	633	8	653	9	674	10
3	746	0	772	0	803	0	828	0
4	1023	1	1055	1	1091	1	1113	1
5	1176	4	1207	4	1247	5	1294	10
6	1251	18	1291	19	1338	20	1369	21
7	1406	0	1465	0	1531	1	1587	7
8	1487	4	1538	6	1601	10	1659	17
9	1551	21	1618	25	1698	31	1771	43
10	3150	0	3232	0	3330	0	3399	1

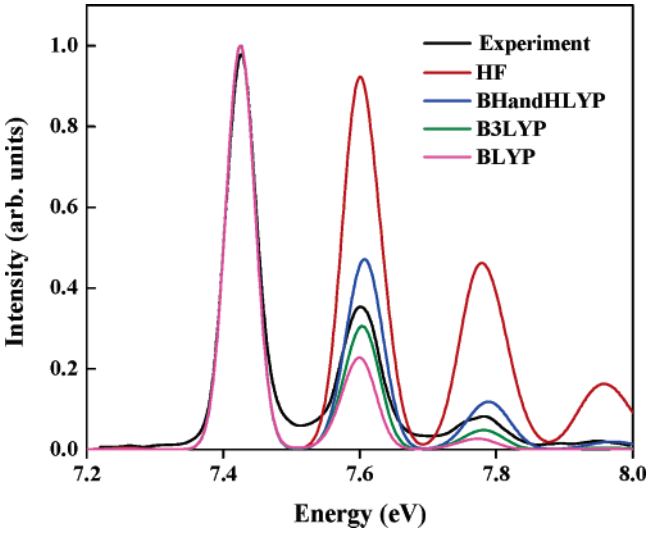

Figure 5. DFT/(HF, BHandHLYP, B3LYP, and BLYP) simulations of the vibrational structure of the first ionization band of anthracene.

the HF estimates is clearly in contradiction with the experimental data.[29] The simulations of the PE spectra indicate that the best agreement between theory and experiment is obtained at the B3LYP level. As an illustrative example, Figure 5 shows the simulated spectrum for the D_0 state (see the Supporting Information for more data) of anthracene using the results derived from the HF and DFT methods. As seen from Figure 5, DFT/BHandHLYP overestimates the intensity of the high-energy vibrational peaks, meaning that BHandHLYP overestimates the hole−vibration coupling constants (and consequently λ_{rel}); in contrast, the BLYP functional underestimates λ_{rel}. The vibrational couplings derived at the HF level completely fail to describe the shape of the experimental band. While the results obtained at the B3LYP level reproduce well the shape of the PE band, the intensity of the second peak is also slightly underestimated. These results suggest that an increase of the EEX amount could lead to a more accurate description of the vibrational couplings. Indeed our calculations indicate that increasing the EEX admixture into the B3LYP functional from 20% to 30% leads to a better agreement between the simulated and the experimental bands (see Supporting Information). Unfortunately, this modification to the functional does not generally lead to an improved description of the excited states. We limit, therefore, our further discussions to the B3LYP results.

The results of the Franck−Condon simulations of the shape of first three PE bands in naphthalene and anthracene using DFT/B3LYP frequencies and Huang−Rhys factors are shown in Figures 6 and 7, respectively. In general, the positions and shapes of the peaks are very well reproduced. The overall agreement between the simulated and the experimental spectra increases the confidence in the reliability of DFT/B3LYP-derived vibronic constants and relaxation energies. The hole−vibrational coupling constants (Huang−Rhys factors) related to the first three PE bands in naphthalene, anthracene, tetracene, and pentacene are shown in Figures 8−11, respectively. In the case of the D_0 states, the main contribution to the relaxation energy comes from high-energy vibrations. The calculations and PE data reveal, however, a significant redistribution of the excited-state relaxation energy toward lower-frequency vibrations. In naphthalene, for instance, the contributions of the high-energy modes over 1200 cm^{-1} account for 95% of the relaxation energy of the D_0 state, while in the excited sates D_1 and D_2 these vibrations account only for 33% and 50% of λ_{rel}, respectively. Accordingly, the contribution of the low-energy

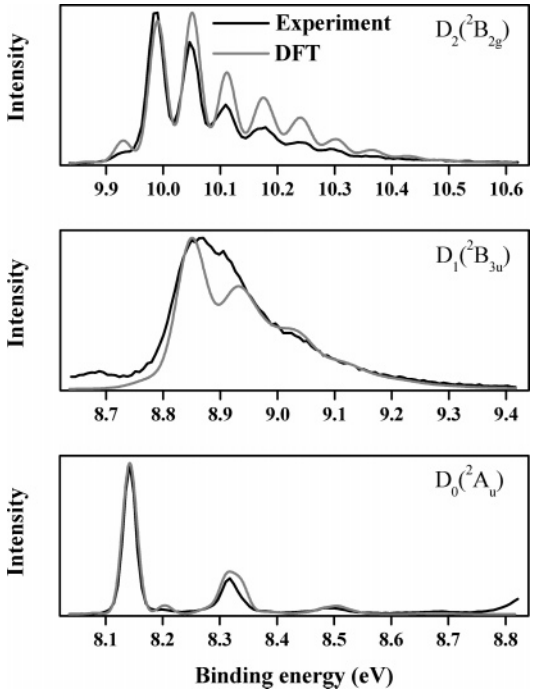

Figure 6. DFT/B3LYP simulations of the vibrational structure of the first three PE bands of naphthalene.

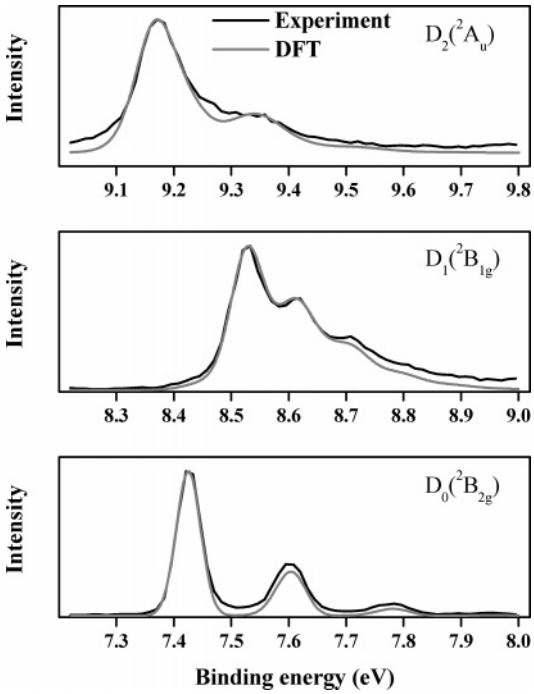

Figure 7. DFT/B3LYP simulations of the vibrational structure of the first three PE bands of anthracene.

modes increases on going from the ground to the second excited radical-cation state. As seen from Figure 8, the lowest-energy, totally symmetric mode at 500 cm^{-1}, in agreement with the experimental observations, is predicted to be particularly active, accounting for about 50% of λ_{rel} in the D_2 state.

The inspection of Figures 8−11 points to a direct correspondence between the nature of the vibronic interaction and (type, vide supra) the electronic-structure pattern of the state. First, as we already mentioned, the hole−vibrational interactions related to first ionization bands (D_0 radical-cation state, i.e., the type I states) are dominated by high-energy vibrations. As seen from Figure 12, λ_{rel} for this group exhibits a linear evolution

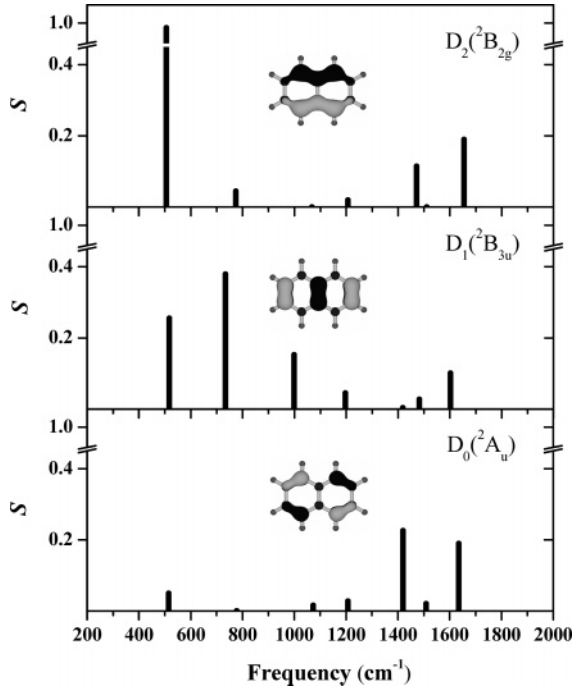

Figure 8. DFT/B3LYP estimates of Huang−Rhys factors, *S*, related to the first three ionization bands of naphthalene.

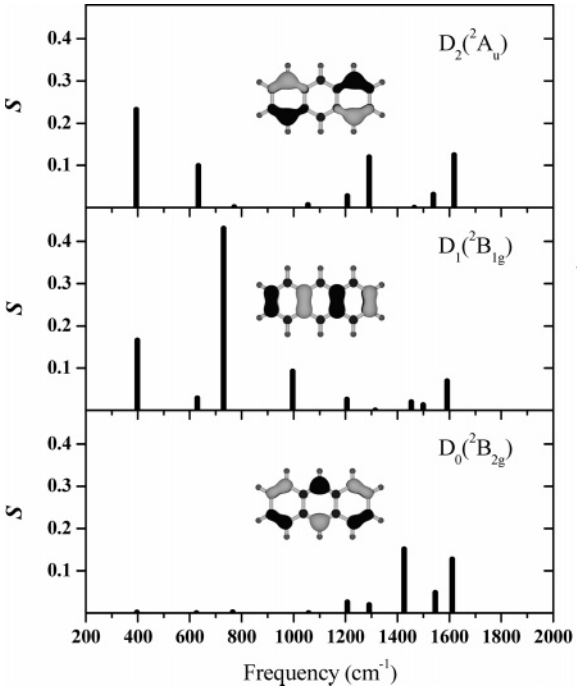

Figure 9. DFT/B3LYP estimates of Huang−Rhys factors, *S*, related to the first two ionization bands of anthracene.

versus the inverse number of carbon atoms. The λ_{rel} of the type II group of states ($^2B_{3u}$ and $^2B_{1g}$ states) exhibits the same linear dependence. As seen from Figures 8−11, the main contribution to the vibrational coupling in this group of states arises from a medium-frequency vibration (depicted in the Supporting Information). The energy of this mode and the corresponding Huang−Rhys factor are comparable along the series ($\omega = 734$ cm^{-1}, $S = 0.38$ in naphthalene; $\omega = 730$ cm^{-1}, $S = 0.44$ in anthracene; $\omega = 738$ cm^{-1}, $S = 0.34$ in pentacene). The vibronic interactions in the third set of states (excited $^2B_{2g}$ and ^2A_u states) come from both low-energy and high-energy vibrations; as the size of the system increases, the relative contribution of the low-

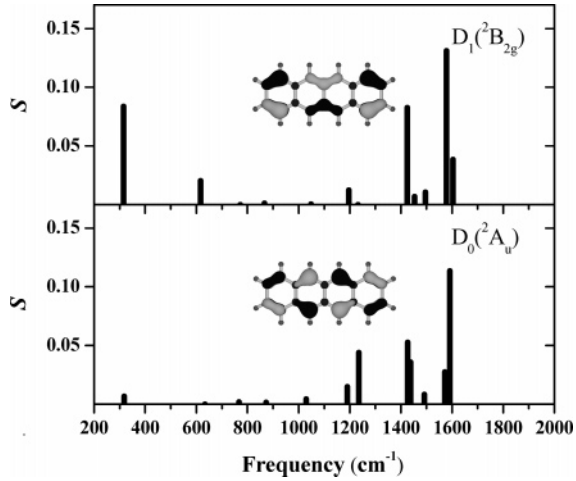

Figure 10. DFT/B3LYP estimates of Huang−Rhys factors, *S*, related to the first two ionization bands of tetracene.

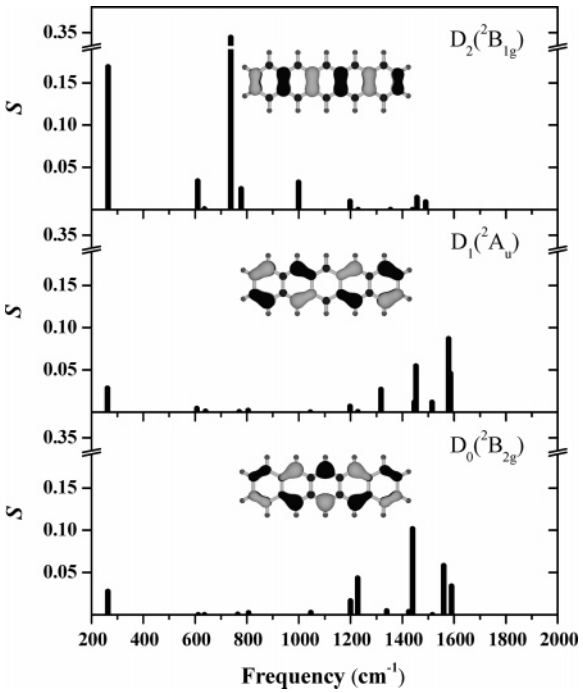

Figure 11. DFT/B3LYP estimates of Huang−Rhys factors, *S*, related to the first three ionization bands of pentacene.

frequency modes drops drastically. The evolution of the relaxation energy of these states as a function of molecular size therefore differs from the linear dependence observed for the other two sets of states.

The pattern of vibronic interactions in a given electronic state can be rationalized in the framework of KT and the concept of orbital vibronic coupling.[43,44] At the KT level of theory, the relaxation energies of the D_0, D_1, and D_2 radical-cation states are equal to the change in orbital energy of the corresponding frontier MOs (Figure 4), which results from the geometry relaxation taking place after ionization. It is then clear that large variations in orbital energies (and thus large vibronic orbital couplings) result from geometry distortions along those vibrational modes that most strongly perturb the bonding/antibonding interactions within the MO. For instance, the strong vibronic interactions with the 1420 and 1635 cm^{-1} vibrational modes in the D_0 state of naphthalene can be explained in the following way. A distortion following the 1420 and 1635 cm^{-1} modes (in the opposite direction or in the same direction as in Figure

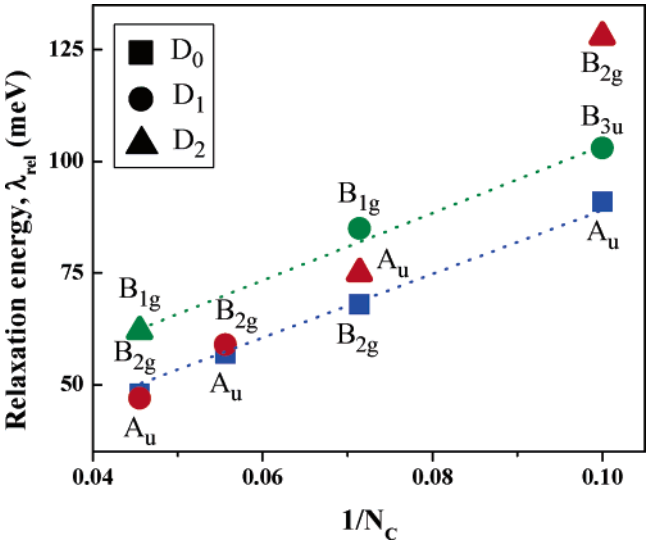

Figure 12. DFT/B3LYP estimates of the relaxation energies, λ_{rel}, of the first three cation states D_0, D_1, and D_2 upon ionization vs the inverse of the number of carbon atoms in naphthalene, anthracene, tetracene, and pentacene. As in Figure 4, the blue, green, and red colors are used to specify the three groups of states according to their type (I, II and III, respectively).

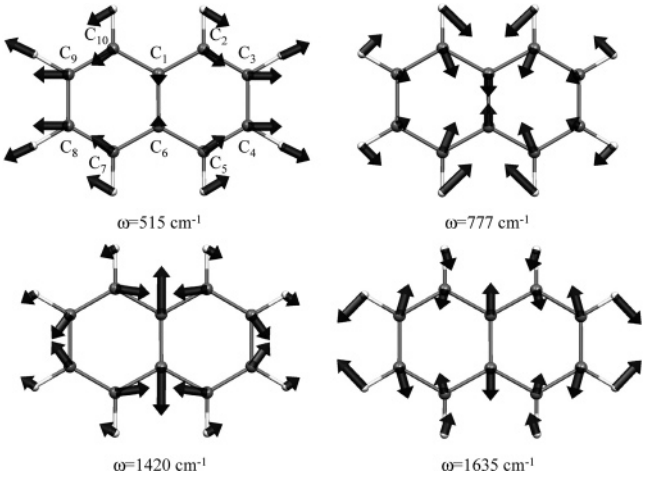

Figure 13. Sketch of the normal modes that yield the largest vibrational couplings in naphthalene.

13 for the 1420 and 1635 cm^{-1} modes, respectively) increases all bonding interactions (C_2-C_3, C_4-C_5, C_7-C_8, and C_9-C_{10}) and decreases all antibonding interactions (C_3-C_4 and C_8-C_9) in the HOMO, thus leading to a significant stabilization of the HOMO orbital energy. A distortion along these two high-energy modes (the patterns and energies of the vibrational modes in the excited D_1 and D_2 states are similar to those in the ground state, D_0; see the Supporting Information) also leads to a significant perturbation of the C_8-C_9, C_6-C_1, and C_4-C_3 bonding interactions present in HOMO − 1. However, while the distortion along the 1635 cm^{-1} (1602 cm^{-1} in D_1) mode leads to in-phase changes of all three bonding interactions, in the case of the 1420 cm^{-1} (1418 cm^{-1} in D_1) mode, the change in the bonding interaction between the C_6 and the C_1 carbons is in opposite phase to those in the C_8-C_9 and C_4-C_3 pairs. As a result, the Huang−Rhys factor for the 1602 cm^{-1} mode in the D_1 state (Figure 8) is significantly larger than that of the 1418 cm^{-1} mode. Both high-frequency modes are also significantly coupled to the HOMO − 2; this is in particular due the strong impact of these modes on the antibonding interaction between the C_6 and C_1 atoms. As seen from Figures 4 and 13, the 515 and 777 cm^{-1} modes do not interact with the HOMO; however, there is a strong coupling between the mode at 777 cm^{-1} (734 cm^{-1} in D_1) and HOMO − 1 and the mode at 515 cm^{-1} (506 cm^{-1} in D_2) and HOMO − 2. The patterns of vibronic interactions in anthracene, tetracene, and pentacene can be rationalized in the same way (see also refs 25−27 and 44 for other examples).

5. Conclusions

We have investigated the structural relaxation in the ground and excited states of naphthalene, anthracene, tetracene, and pentacene that appear after ionization. The photoelectron measurements and DFT calculations show that there is a direct dependence between the nature of the vibronic interaction and the pattern of the electronic structure. Our results reveal that while in the case of ground cation states the main contribution to relaxation energy comes from high-energy vibrations the excited-state relaxation energies show a significant redistribution toward lower-frequency vibrations.

We have also evaluated how the amount of exact Hartree−Fock exchange included in the hybrid functionals affects the DFT results. We have shown that, among the standard functionals, B3LYP provides the best description of geometry modifications upon ionization in oligoacenes for both ground and excited states.

Acknowledgment. This paper is dedicated to Professor Robert Silbey on the occasion of his 65th birthday. For over 25 years, Bob has been a continuous source of inspiration and has had a tremendous impact on the way computational chemistry is carried out in our group. We are proud to be Bob's students and collaborators and to carry on his legacy of theory for experimentalists. The authors thank S. L. Sörensen (Lund University, Sweden) and M. Tschaplyguine (Uppsala University and MAX-Lab, Lund, Sweden) for experimental help. The work at Georgia Tech is partly supported by the National Science Foundation, through the Science and Technology Center for Materials and Devices for Information Technology Grant No. DMR-0120967, Chemistry Research Instrumentation and Facilities Award No. CHE-0443564, and Grant No. CHE-0343321. Research in Linköping in general is supported by the Swedish Science Foundation, the Swedish Foundation for Strategic Research through the Center for Advanced Molecular Materials, the Center for Organic Electronics, the Commission of the European Union through the Integrated Project NAIMO (Grant No. NMP4-CT-2004-500355), and contracts with DuPont Corporation, U. S., and Merck Chemicals, U. K.

Supporting Information Available: Calculated relaxation energies and Huang−Rhys factors of naphthalene, anthracene, tetracene, and pentacene not shown in the text, a sketch of the vibrational modes, and the fitting of the second and third ionization bands in anthracene. This material is available free of charge via the Internet at http://pubs.acs.org.

References and Notes

(1) Salama, F.; Allamandola, L. J. *J. Chem. Phys.* **1991**, *94*, 6964.

(2) Hudgins, D. M.; Allamandola, L. J. *J. Phys. Chem.* **1995**, *99*, 8978.

(3) Biennier, L.; Salama, F.; Allamandola, L. J.; Scherer, J. J. *J. Chem. Phys.* **2003**, *118*, 7863.

(4) Le Page, V.; Keheyan, Y.; Snow, T. P.; Bierbaum, V. M. *J. Am. Chem. Soc.* **1999**, *121*, 9435.

(5) Sukhorukov, O.; Staicu, A.; Diegel, E.; Rouille, G.; Henning, T.; Huisken, F. *Chem. Phys. Lett.* **2004**, *386*, 259.

(6) Zhao, L.; Lian, R.; Shkrob, I. A.; Crowell, R. A.; Pommeret, S.; Chronister, E. L.; Liu, A. D.; Trifunac, A. D. *J. Phys. Chem. A* **2004**, *108*, 25.
(7) Bendikov, M.; Wudl, F.; Perepichka, D. F. *Chem. Rev.* **2004**, *104*, 4891.
(8) Brédas, J. L.; Beljonne, D.; Coropceanu, V.; Cornil, J. *Chem. Rev.* **2004**, *104*, 4971.
(9) Katz, H. E.; Bao, Z. N.; Gilat, S. L. *Acc. Chem. Res.* **2001**, *34*, 359.
(10) Deng, W. Q.; Goddard, W. A. *J. Phys. Chem. B* **2004**, *108*, 8614.
(11) Troisi, A.; Orlandi, G. *J. Phys. Chem. B* **2005**, *109*, 1849.
(12) Payne, M. M.; Parkin, S. R.; Anthony, J. E. *J. Am. Chem. Soc.* **2005**, *127*, 8028.
(13) Payne, M. M.; Parkin, S. R.; Anthony, J. E.; Kuo, C.-C.; Jackson, T. N. *J. Am. Chem. Soc.* **2005**, *127*, 4986.
(14) Dierksen, M.; Grimme, S. *J. Chem. Phys.* **2004**, *120*, 3544.
(15) Dierksen, M.; Grimme, S. *J. Phys. Chem. A* **2004**, *108*, 10225.
(16) Zgierski, M. Z. *J. Chem. Phys.* **1986**, *85*, 109.
(17) Negri, F.; Zgierski, M. Z. *J. Chem. Phys.* **1993**, *99*, 4318.
(18) Negri, F.; Zgierski, M. Z. *J. Chem. Phys.* **1996**, *104*, 3486.
(19) Negri, F.; Zgierski, M. Z. *J. Chem. Phys.* **1997**, *107*, 4827.
(20) Cockett, M. C. R.; Ozeki, H.; Okuyama, K.; Kimura, K. *J. Chem. Phys.* **1993**, *98*, 7763.
(21) Andruniow, T.; Pawlikowski, M. *Chem. Phys.* **1998**, *236*, 35.
(22) Andruniow, T.; Pawlikowski, M. *Chem. Phys.* **1998**, *236*, 25.
(23) Andrews, L.; Friedman, R. S.; Kelsall, B. J. *J. Phys. Chem.* **1985**, *89*, 4016.
(24) Andrews, L.; Kelsall, B. J.; Blankenship, T. A. *J. Phys. Chem.* **1982**, *86*, 2916.
(25) Kato, T.; Yamabe, T. *J. Chem. Phys.* **2001**, *115*, 8592.
(26) Kato, T.; Kondo, M.; Yoshizawa, K.; Yamabe, T. *Synth. Met.* **2002**, *126*, 75.
(27) Kato, T.; Yoshizawa, K.; Yamabe, T. *Chem. Phys. Lett.* **2001**, *345*, 125.
(28) Gruhn, N. E.; da Silva, D. A.; Bill, T. G.; Malagoli, M.; Coropceanu, V.; Kahn, A.; Brédas, J. L. *J. Am. Chem. Soc.* **2002**, *124*, 7918.
(29) Coropceanu, V.; Malagoli, M.; da Silva, D. A.; Gruhn, N. E.; Bill, T. G.; Brédas, J. L. *Phys. Rev. Lett.* **2002**, *89*, 275503.
(30) Malagoli, M.; Coropceanu, V.; da Silva, D. A.; Brédas, J. L. *J. Chem. Phys.* **2004**, *120*, 7490.
(31) da Silva, D. A.; Friedlein, R.; Coropceanu, V.; Öhrwall, G.; Osikowicz, W.; Suess, C.; Sorensen, S. L.; Svensson, S.; Salaneck, W. R.; Brédas, J. L. *Chem. Commun.* **2004**, 1702.
(32) Szczepanski, J.; Drawdy, J.; Wehlburg, C.; Vala, M. *Chem. Phys. Lett.* **1995**, *245*, 539.
(33) Szczepanski, J.; Vala, M.; Talbi, D.; Parisel, O.; Ellinger, Y. *J. Chem. Phys.* **1993**, *98*, 4494.
(34) Yamane, H.; Nagamatsu, S.; Fukagawa, H.; Kera, S.; Friedlein, R.; Okudaira, K. K.; Ueno, N. *Phys. Rev. B* **2005**, *72*.
(35) Frisch, M. J.; Trucks, G. W.; Schlegel, H. B.; Scuseria, G. E.; Robb, M. A.; Cheeseman, J. R.; Zakrzewski, V. G.; Montgomery, J. A., Jr.; Stratmann, R. E.; Burant, J. C.; Dapprich, S.; Millam, J. M.; Daniels, A. D.; Kudin, K. N.; Strain, M. C.; Farkas, O.; Tomasi, J.; Barone, V.; Cossi, M.; Cammi, R.; Mennucci, B.; Pomelli, C.; Adamo, C.; Clifford, S.; Ochterski, J.; Petersson, G. A.; Ayala, P. Y.; Cui, Q.; Morokuma, K.; Malick, D. K.; Rabuck, A. D.; Raghavachari, K.; Foresman, J. B.; Cioslowski, J.; Ortiz, J. V.; Stefanov, B. B.; Liu, G.; Liashenko, A.; Piskorz, P.; Komaromi, I.; Gomperts, R.; Martin, R. L.; Fox, D. J.; Keith, T.; Al-Laham, M. A.; Peng, C. Y.; Nanayakkara, A.; Gonzalez, C.; Challacombe, M.; Gill, P. M. W.; Johnson, B. G.; Chen, W.; Wong, M. W.; Andres, J. L.; Head-Gordon, M.; Replogle, E. S.; Pople, J. A. *Gaussian 98*, revision A.11; Gaussian, Inc.: Pittsburgh, PA, 1998.
(36) Reimers, J. R. *J. Chem. Phys.* **2001**, *115*, 9103.
(37) Bally, T.; Carra, C.; Fülscher, M. P.; Zhu, Z. D. *J. Chem. Soc., Perkin Trans. 2* **1998**, 1759.
(38) Brundle, C. R.; Robin, M. B.; Keubler, N. A. *J. Am. Chem. Soc.* **1972**, *94*, 1466.
(39) Brogli, F.; Heilbronnner, E.; Kobayashi, T. *Helv. Chim. Acta* **1972**, *55*, 274.
(40) Boschi, R.; Murrell, J. N.; Schmidt, W. *Faraday Discuss.* **1972**, 116.
(41) Schmidt, W. *J. Chem. Phys.* **1977**, *66*, 828.
(42) Koopmans, T. *Physica* **1934**, *1*, 104.
(43) Bersuker, I. B. *Chem. Rev.* **2001**, *101*, 1067.
(44) Kato, T.; Yamabe, T. *J. Chem. Phys.* **2003**, *119*, 11318.